

Graphene-Based Planar Microstrip Patch Antenna with Circular Polarization Capability

Maryam Yaghobi¹, Pejman Rezaei¹ and Mohammad M. Fakharian²

Abstract— In this paper, a graphene-based patch antenna structure is designed. Due to the use of graphene, the design of the antenna is directly related to its chemical potential. The structure of this paper is developed from constant chemical potential (μ_c) to control the polarization of the antenna, which can provide a specific radiation behavior for the field around the antenna. Therefore, the possibility of achieving an antenna with optimal adaptation in the frequency range of 2 to 4 THz with resonant frequency 3.2 THz and return loss in the range of 2.9 to 4 THz has been investigated. In addition, the possibility of creating antenna polarization with constant potential in two modes of right and left-hand circular polarization has been investigated. At around the 3 THz frequency range, an axial ratio of less than 3 dB is obtained. For the frequency range of 2.9 to 3.05 THz, the polarization is achieved in RHCP and LHCP modes. The method for attaining circular polarization is to add circular layers at the edges of the structure antenna. A considerable bandwidth can be obtained with this technique.

Index Terms— Terahertz, Graphene surface conductivity, Microstrip antenna, Circular polarization.

I. INTRODUCTION

Increasing bit rate and consequently bandwidth increment, as the demand of today's telecommunications, research motivates towards higher frequencies, THz, infrared, and optics [1,2]. Redesign of communication devices known in the microwave, such as antennas [3-8], filter [9,10], switches [11,12], sensor [13,14], multiplexer [15,16], absorber [17-21] and etc, is a requirement of this process.

Researchers in recent years have been fascinated by the unique properties of two-dimensional plasmonic materials such as graphene. Because graphene, like other carbon structures such as diamonds, graphite, and graphene tubes, has high thermal conductivity, it is composed of one element compared to other two-dimensional materials. Graphene, with suitable electronic transmission properties, is used to design various plasmonic structures. Graphene is considered the thinnest layer (0.335 nm thick), a honeycomb lattice with a width of one carbon atom, which is an elastic material [22]. Graphene material has attracted much attention due to its valuable optical, electrical, magnetic, mechanical, and thermal properties [23, 24].

With the realization of the elastic surface resistance properties of graphene, widely used in many devices, including

antennas, waveguides, resonators, filters, multiplexers, absorbers, modulators. Recently, many graphene-based antennas have been proposed, such as Yagi-Uda, leakage wave, the reconfigurable antenna [25, 26], graphene antennas have shown broad capabilities in the terahertz band.

The parasitic elements are tuned using potential chemical changes in the graphene-based Yagi-Uda antenna [21]. In [27], a filtered pseudo-Yagi antenna (FIQYA) is implemented using graphene. Graphene bipolar antennas have been used to generate more accurate beams to improve the Yagi-Uda (PCA) graphene antenna. A graphene optical antenna is used to implement amplified biomolecular detection [26].

Near the light field, two graphene-based antennas [28] describe the light in the THz region. The THz graphene antenna, UT-shaped, in [29], to announce a plasmonic platform, in [30], an optically conductive antenna, by using spatially dispersed graphene nanoribbons (GNPs) to maximize conductivity, is shown. Graphene fingerprint transistors for understanding a THz multi-element sensor for multi-pixel parallel detection are described in [31]. In [32], the realization of broadband antennas based on the negative differential resistance characteristic of the transistor, the graphene field-effect (GFET), is investigated. In [33], a graphene leak antenna that can reconfigure the LWA radiation pattern over a wide frequency range in the terahertz band is proposed.

In this paper, the proposed antenna is designed to create circular polarization in graphene patch antennas, which can create circular polarization in two modes of right-hand circular polarization and left-hand circular polarization with an axial ratio of less than 3 dB at 3 THz. We know that circular polarization occurs when two orthogonal field components are excited by phase differences [22], and circular polarization antennas are suitable when multidirectional interference and wave reflection are problematic.

Several techniques for obtaining the circular polarization behavior of microstrip antennas, including single-feed and double-feed schemes, have been reported. The microstrip antenna design with circular polarization with a single power supply includes a square piece with shortened corners, a diagonal slit and adding to the diagonal corners [23, 24] and a U slot, and so on. The proposed physical structure of the antenna is a square ring with a rectangular patch filled with internal graphene in which a graphene ring is added at the diagonal edges of the inner patch.

1: Electrical and Computer Engineering Faculty, Semnan University, Semnan, Iran

2: Faculty of Engineering, University of Garmsar, Garmsar, Iran

Corresponding author: fakharian@fimgarmsar.ac.ir

II. ELECTROMAGNETIC BEHAVIOR OF GRAPHENE

The surface conductivity of graphene (σ), using the Kobo formula [21, 34] can be expressed as follows:

$$\sigma(\omega) = -\frac{e^2 E_F}{\pi h^2} \frac{i}{\omega - i\Gamma^{-1}} + \frac{e^2}{4h} \left\{ \theta(h\omega - 2E_F) - \frac{i}{\pi} \ln \left| \frac{h\omega - 2E_F}{h\omega + 2E_F} \right| \right\} \quad (1)$$

Where $\tau = \Gamma$ and $\theta(t)$ is the Heaviside step function. The amount of energy required by an electron to transfer from one layer to another of graphene is extracted from ($E_F = 100$ mv). The first period in Equation (1) is similar to the Droid model for metals and has an internal bond effect. The second period of Equation (2) shows the impact of the middle band, which depends more on the absorption losses.

The surface conductivity of graphene can be electromagnetically modeled by the tensor [35, 36], shown in the following [3].

$$\sigma(\omega, E_F, \Gamma, T) = \frac{ie^2(\omega - i\Gamma)}{\pi h^2} \left\{ \frac{1}{(\omega - i\Gamma)^2} \int_0^\infty \varepsilon \left(\frac{\partial f_d(\varepsilon)}{\partial \varepsilon} - \frac{\partial f_d(-\varepsilon)}{\partial \varepsilon} \right) \partial \varepsilon - e^{-j\omega t} \int_0^\infty \frac{f_d(-\varepsilon) - f_d(\varepsilon)}{(\omega - i\Gamma)^2 - 4\left(\frac{\varepsilon}{h}\right)^2} \right\} \quad (2)$$

Where h is the Planck constant, e is the electron charge, the Fermi energy level of the graphene layer, Γ is the phenomenological constant of the dispersion rate at the graphene surface, and T is the temperature of the graphene layer. In Equation (3), the ($f_d(\varepsilon)$) function is the Fermi-Dirac distribution [5]:

$$f_d(\varepsilon) = \frac{1}{e^{(\varepsilon - E_F)/k_B T} + 1} \quad (3)$$

Where is the K_B Boltzmann constant? In Equation (2), the approximate derivative $\frac{\partial f_d(\varepsilon)}{\partial \varepsilon}$ is substituted for the actual possible difference of the electrons in the conduction or band peak $f_d(\varepsilon + d\varepsilon) - f_d(\varepsilon)$, indicating the intermediate band transfer probability. The first integral in Equation (2) represents the contribution of the intra-band transition, while the second is due to the low-band effect.

The volumetric friction coefficient equivalent to the graphene layer in Equation (4) can be obtained from the following Equation [5]:

$$\epsilon_r = 1 + \frac{\sigma(\omega)}{i\omega \Delta \epsilon_0} \quad (4)$$

Where Δ is the adequate thickness of the graphene layer, in the extraction of Equation (4), it is assumed that its thickness is small enough that the flow is uniformly distributed along with the thickness. The volumetric model introduced here is the same size as the $\Delta < 1$ nm level model.

III. RESULTS AND STRUCTURE OF GRAPHENE-BASED MICROSTRIP ANTENNA

The configuration of the graphene patch antenna is shown in Fig. 1 In this paper, one method of adding an extra section to

the edges of a patch is used to provide circular polarization. The structure of the antenna is designed on a substrate with a dielectric constant of 3.8. The substrate with thickness H is placed on the ground. According to the following Figure, the antenna base consists of a patch with dimensions and an internal patch of graphene with dimensions and a circular ring in diagonal corners with outer diameter c and inner diameter a . The dimensions of the proposed antenna are shown in Table (1).

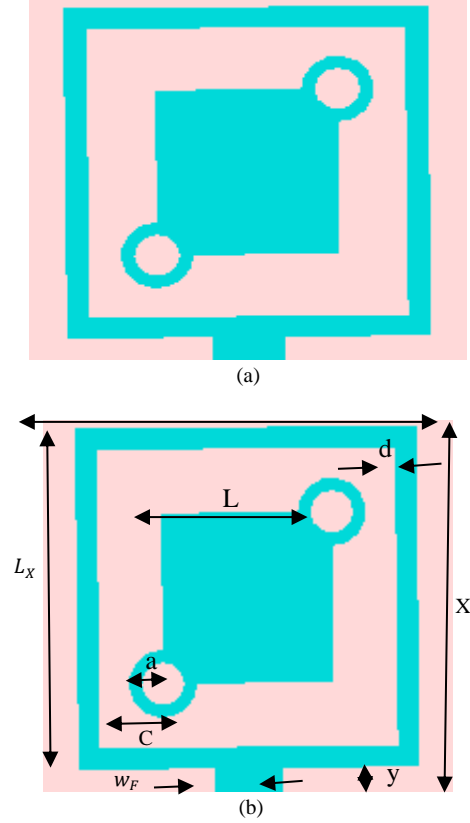


Fig. 1. Antenna structure (a) LHCP (b) RHCP.

Simulations are implemented using CST Microwave Studio. The microstrip antenna is designed with circular polarization using diagonal edges. Boundary condition settings are defaulted by CST software that displays the structure in a colored cube. The colors of the faces vary according to the type of boundary condition defined, which applied the boundary conditions of electric and magnetic fields, etc.

TABLE I
The Dimensions Of The Proposed Antenna

Variable	Value (mm)
d	5
L_x	40
X	160
L	40
a	10
w_F	10
c	16
y	40

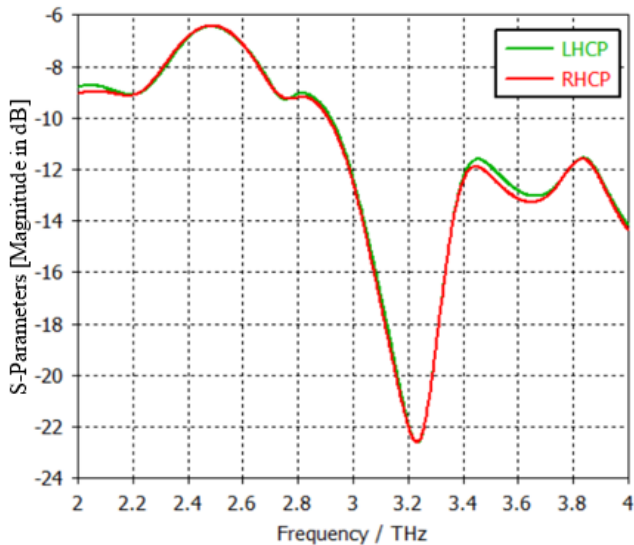


Fig. 2. Antenna S_{11} parameter diagram.

In Fig. 2, the parameter S_{11} diagram of the antenna is shown. Antenna adaptation at 3 THz has good conditions for polarization in RHCP, LHCP antenna modes. In general, the matching requirements of patch antennas at return losses are acceptable for adaptation in the range below 10 dB.

The axial polarization ratio of the antenna at the central frequency and the range of antenna application are shown in Fig. 3.

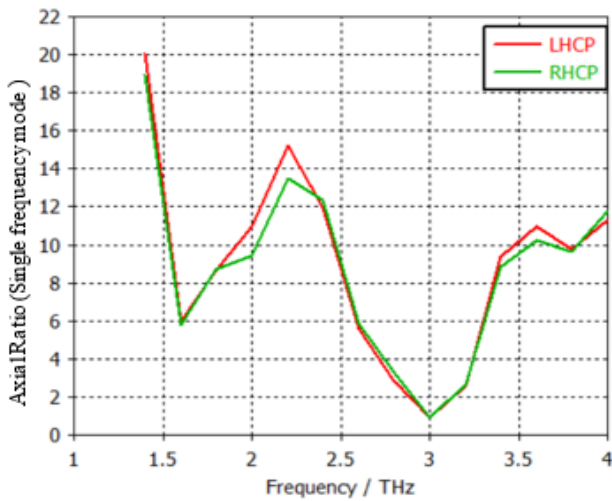


Fig. 3. Antenna axial ratio (a) RHCP (b) LHCP at 3 THz.

The axial ratio below 3 dB indicates the desired polarization in RHCP and LHCP modes. The efficiency of this proposed antenna is also shown in Fig. 4. As from the antenna's efficiency diagram is apparent, the cost of providing RHCP and LHCP simultaneously in the antenna topology is slightly lowering than its efficiency. According to Fig. 4, it is observed that the maximum radiation efficiency at the frequency of 4 THz, 85%. In the range shown, the lowest radiation efficiency is 52% at frequency 2 THz, and in the range

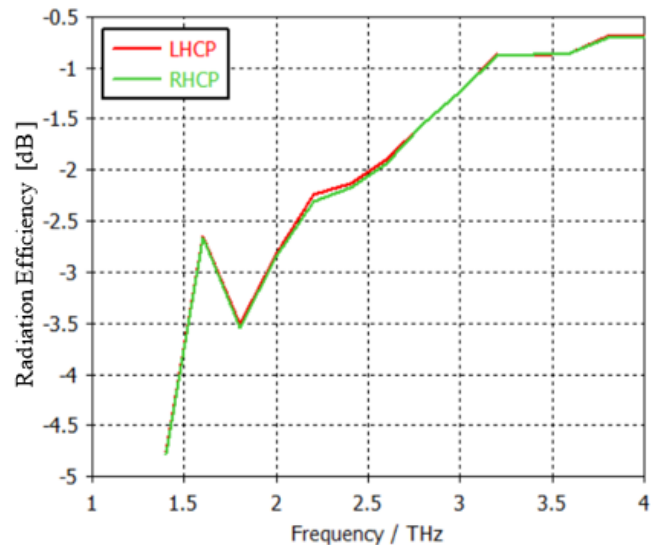


Fig. 4. The radiation efficiency of the proposed antenna.

1.89 to 2.49 THz, it is higher than 70%, and at the mentioned frequency of 3 THz, it shows 74% efficiency.

The E-plane and H-plane radiation patterns in the proposed antenna for RHCP and LHCP at the center frequency of 3 THz with the maximum gain are shown in Fig. 5 and 6.

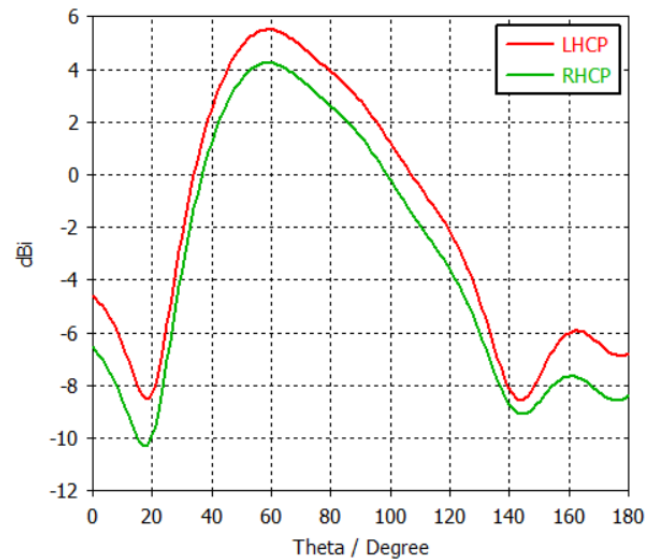


Fig. 5. E-plane radiation pattern of proposed antenna in RHCP and LHCP mode at 3 THz.

The current distribution in the designed antenna changes so that the result is two orthogonal electric fields with a phase difference of $\pm 90^\circ$. The E-field and H-field distributions of antennae for LHCP and RHCP radiation modes are visible in Fig. 7 and 8.

Fig. 7 and 8 show the antenna's E-field and H-field distribution profiles for RHCP and LHCP in the center frequency, respectively. As this Figure shows, the diameter of the diagonal edges is different from other surfaces. This difference is set to provide CP in the antenna far-field.

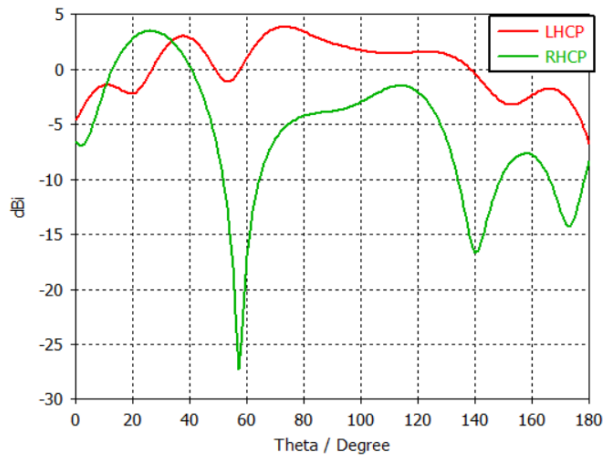


Fig. 6. H-plane radiation pattern of proposed antenna in RHCP and LHCP mode at 3 THz.

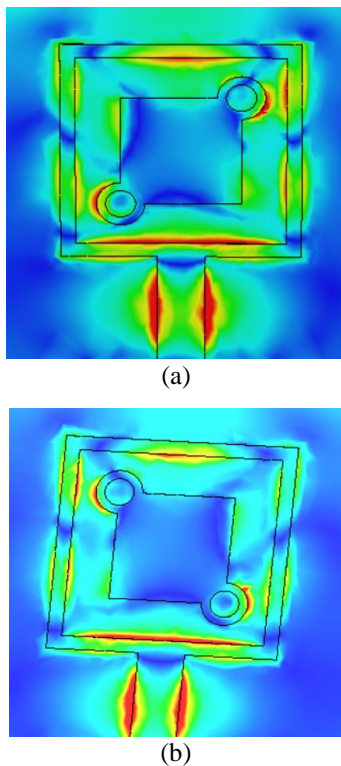


Fig. 7. The E-field distribution of the proposed antenna at 3 THz. (a) LHCP, (b) RHCP.

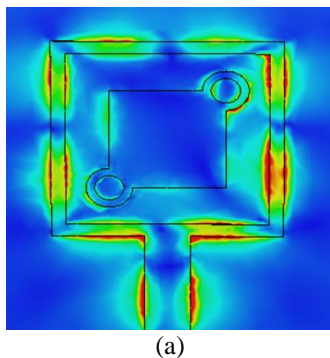


Fig. 8. The H-field distribution of the proposed antenna at 3 THz. (a) LHCP, (b) RHCP.

IV. CONCLUSION

In this work, a graphene-based microstrip patch antenna is designed with a polarization control function. The properties of graphene are used to create circular antenna polarization. The antenna structure is designed to achieve RHCP and LHCP through the Fermi energy level in graphene, where the adaptation of the antenna in the frequency range of 3 THz has good conditions for the polarization mode in the antenna. The obtained axial ratio below 3 dB indicated a proper circular polarization for the frequency range of 2.9 to 3.05 THz, and the polarization is achieved in RHCP and LHCP modes. However, due to the antenna's variety of active radiation elements in each polarization, the efficiency is partly affected by different operating methods and radiating edge levels. The return loss in the operating range (2.9-4 THz) was more than 10 dB with good adaptation behavior. Changes in the energy level of graphene Fermi can directly affect the antenna. The structure of the designed antenna with a constant chemical potential was investigated, and finally, we achieved control of the circular polarization of the antenna. This goal will be explored in future research to adjust the chemical potential.

ACKNOWLEDGMENT

The authors would like to thank the support from Semnan University. The authors would like to thank the journal editor and reviewers for their valuable comments.

REFERENCES

- [1] Choi JH. High-speed devices and circuits with THz applications., CRC Press (2015).
- [2] Pereira, M. F., and Shulika, O. (Eds.), Terahertz and mid-infrared radiation: generation, detection, and applications. Springer, (2011).
- [3] M. Jafari Chashmi, P. Rezaei, and N. Kiani, Y-shaped graphene-based antenna with switchable circular polarization, *Opt. -Int. J. Light Electron. Opt.* 200 (2020), 163321.
- [4] P. Sohrabi, P. Rezaei, S. Kiani, and M. Fakhr, "A symmetrical SIW-based leaky-wave antenna with continuous beam scanning from backward-to-forward through broadside," *Wireless Networks*, vol. 27, pp. 5417-5424, Nov. 2021.
- [5] M. Jafari Chashmi, P. Rezaei, and N. Kiani, Polarization controlling of multi resonant graphene-based microstrip antenna, *Plasmonics* 15 (2) (2020) 417-426.

- [6] N. Kiani, F. Tavakkol Hamedani, and P. Rezaei, Polarization controlling idea in graphene-based patch antenna, *Optik* 239 (2021) 166795.
- [7] M. Jafari Chashmi, P. Rezaei, and N. Kiani, Reconfigurable graphene-based V-shaped dipole antenna: from quasi-isotropic to directional radiation pattern, *Optik Int. J. Light Electron. Opt.* 184 (2019) 421-427.
- [8] N. Kiani, F. Tavakol Hamedani, and P. Rezaei, Polarization controlling method in reconfigurable graphene-based patch four-leaf clover-shaped antenna, *Optik Int. J. Light Electron. Opt.* 231 (2021), 166454.
- [9] Khani S, Danaie M, and Rezaei P, Size reduction of MIM surface plasmon-based optical bandpass filters by the introduction of arrays of silver nanorods. *Physica E: Low-dimensional Systems and Nanostructures*, (2019), 113, 25-34.
- [10] S. Kiani, P. Rezaei, and M. Fakhr, An overview of interdigitated microwave resonance sensors for liquid samples permittivity detection, in *Interdigital Sensors: Progress over the last two decades*, Springer, 2021.
- [11] Khani, S., Danaie, M., and Rezaei, P, All-optical plasmonic switches based on asymmetric directional couplers incorporating Bragg gratings, (2020), *Plasmonics*, 15(3), 869-879.
- [12] Khani, S., Danaie, M., and Rezaei, P, Compact and low-power all-optical surface plasmon switches with isolated pump and data waveguides and a rectangular cavity containing nano-silver strips. *Superlattices and Microstructures*, vol. 141, pp. 106481, 2020.
- [13] Ghods, M. M., and Rezaei, P, Graphene-based Fabry-Perot resonator for chemical sensing applications at mid-infrared frequencies. *IEEE Photonics Technology Letters*, (2018), 30(22), 1917-1920.
- [14] S. Kiani, P. Rezaei, and M. Navaei, "Dual-sensing and dual-frequency microwave SRR sensor for liquid samples permittivity detection, *Measurement*, vol. 160, pp. 107805, Aug. 2020.
- [15] Chen, J, A broadband wavelength demultiplexer assisted by SWG-based directional couplers, (2020), *Optik*, 202, 163602.
- [16] Khani, S, Danaie, M, and Rezaei, P, Double and triple-wavelength plasmonic demultiplexers based on improved circular nanodisk resonators. *Optical Engineering*, (2018), 57(10), 107102.
- [17] Zamzam, P., Rezaei, P., and Khatami, S. A, Quad-band polarization-insensitive metamaterial perfect absorber based on bilayer graphene metasurface. *Physica E: Low-dimensional Systems and Nanostructures*, (2021), 128, 114621.
- [18] Ghods MM, and Rezaei P, Ultra-wideband microwave absorber based on uncharged graphene layers, *Electromagnetic waves, and applications.*, *J. Electromag*, (2017), *Wav. Appl.*, vol. 32, no. 15, pp. 1950-1960.
- [19] Razani, A. N., and Rezaei, P, Multiband Polarization Insensitive and Tunable Terahertz Metamaterial Perfect Absorber Based on The Heterogeneous Structure of Graphene, (2021).
- [20] Zamzam P, and Rezaei P, A terahertz dual-band metamaterial perfect absorber based on metal-dielectric-metal multi-layer columns., *Optic. Quant. Electron.*, (2021), vol. 53, pp. 109.
- [21] A. Norouzi Razani, and P. Rezaei, "Broadband polarization-insensitive and tunable terahertz metamaterial perfect absorber based on the graphene disk and square ribbon," *Superlattices and Microstructures*, Early Access, 2022.
- [22] Sikdar, D., Zhu, W., Cheng, W., and Premaratne, M, Substrate-mediated broadband tunability in plasmonic resonances of metal nanoantennas on finite high-permittivity dielectric substrate, (2015), *Plasmonics*, 10(6), 1663-1673.
- [23] Liu H, Sun S, Wu L, and Bai P, Optical near-field enhancement with graphene bowtie antennas. *Plasmonics*, vol. 9, no. 4, pp. 845-850, 2014.
- [24] Zhu B., Ren G., Gao Y., Wu B., Lian Y., and Jian S, Creation of graphene plasmons vortex via cross shape nanoantennas under linearly polarized incidence. *Plasmonics*, vol. 12, no. 3, pp. 863-868, 2017.
- [25] Ekşioğlu Y, Cetin AE, and Durmaz H, Multi-band plasmonic platform utilizing UT-shaped graphene antenna arrays. *Plasmonics*, (2018), vol. 13, no. 3, pp. 1081-1088.
- [26] Computer Simulation Technology (CST), CST Microwave Studio Ver. 2015. www.cst.com.
- [27] Hanson GW, Dyadic Green's functions and guided surface waves for a surface conductivity model of graphene. *J. Appl. Phys.*, (2008), vol. 103, pp. 064302.
- [28] Slepyan GY, Maksimenko SA, Lakhtakia A, Yevtushenko O, and Gusakov AV, Electrodynamics of carbon nanotubes: Dynamic conductivity, impedance boundary conditions, and surface wave propagation. *Phys.*, (1999), *Rev. B*, vol. 60, pp. 17136.
- [29] Hanson GW, Dyadic Green's functions for an anisotropic, non-local model of biased graphene. *IEEE Trans. Antennas Propag.*, (2008), vol. 56, no. 3, pp. 747-757.
- [30] Emadi R, Emadi H, Emadi R, Safian R, and Nezhad AZ, Analysis and design of photoconductive antenna using spatially dispersive graphene strips with parallel-plate configuration. *IEEE J. Selected Topics in Quant. Electron.*, (2017), vol. 24, no. 2, pp. 1-9.
- [31] Bianco F, Miseikis V, Perenzoni D, Coletti C, Perenzoni M, and Tredicucci A, Antenna-coupled graphene field-effect transistors as a terahertz imaging array. *IEEE Trans. Terahertz Sci. Technol.*, (2020), *11(1)*, 70-78.
- [32] Tian J, Nagarkoti, DS, Rajab KZ, and Hao Y, High-impedance surface loaded with graphene non-foster circuits for low-profile antennas. *IEEE Antennas Wirel. Propag. Lett.*, (2017), vol. 16, pp. 2655-2658.
- [33] Li J, He, M., Wu, C., and Zhang, C, Radiation-pattern-reconfigurable graphene leaky-wave antenna at terahertz band based on dielectric grating structure. *IEEE Antennas and Wireless Propagation Letters*, (2017), 16, 1771-1775.
- [34] Wu Y, Qu M, Jiao L, and Liu Y, Tunable terahertz filter-integrated quasi-Yagi antenna based on graphene. *Plasmonics*, (2017), 12(3):811-817.
- [35] Giddens H, Yang L, Tina J, and Hao Y, Mid-infrared reflect-array antenna with beam switching enabled by continuous graphene layer. *IEEE Photon Technol Lett.*, (2018), 30(8):748-751.
- [36] Fuscaldo W, Burghignoli P, Baccarelli P, and Galli A, Graphene Fabry-Perot cavity leaky-wave antennas: plasmonic versus nonplasmonic solutions. *IEEE Trans Antennas Propag.*, (2017), 65(4):1651-1660.